RSC Advances

PAPER

Cite this: *RSC Adv.*, 2020, **10**, 8866

Efficient fluorescent OLEDS based on assistant acceptor modulated HLCT emissive state for enhancing singlet exciton utilization†

Jayaraman Jayabharathi,* Jagathratchagan Anudeebhana, Venugopal Thanikachalam and Sekar Sivaraj

Received 21st January 2020
Accepted 20th February 2020

DOI: 10.1039/d0ra00658k

rsc.li/rsc-advances

Phenylamine phenanthroimidazole based bipolar compounds with donor–acceptor (D–A) architecture namely, 4-(1-(2,3-dihydrobenzo[*b*][1,4]dioxin-5-yl)-6,9-di(pyren-4-yl)-1*H*-phenanthro[9,10-*d*]imidazol-2-yl)-*N*,*N*-diphenylaniline (DDPPPA) and 4′-(1-(2,3-dihydrobenzo[*b*][1,4]dioxin-5-yl)-6,9-di(pyren-4-yl)-1*H*-phenanthro[9,10-*d*]imidazol-2-yl)-*N*,*N*-diphenyl-[1,1′-biphenyl]-4-amine (DDPBA) have been synthesized with highly fluorescent pyrene moieties at C6- and C9-positions. The C6 and C9 modification enhanced the thermal, photochemical and electroluminescent properties. Both molecules were employed as blue emitters in non doped organic light emitting devices (OLEDs) and show high performances due to hybridized local and charge-transfer properties. An OLED with DDPPPA/DDPBA emissive layer shows deep-blue emission with maximum external quantum efficiency (η_{ex}), current efficiency (η_c) and power efficiency (η_p) of 5.7/6.0%, 10.5/12.0 cd A^{-1} and 8.3/9.2 lm W^{-1}, respectively. Both devices show high singlet exciton utilizing efficiency (η_s) of DDPPPA-31.33% and DDPBA-35.29%. The doped device *m*-MTDATA:DDPPPA/*m*-MTDATA:DDPBA shows maximum efficiencies of η_c −7.4/8.23 cd A^{-1}; η_p −5.8/6.13 lm W^{-1}; η_{ex} −4.72/5.63% (5 wt%):η_c −8.36/9.15 cd A^{-1}; η_p −6.32/6.65 lm W^{-1}; η_{ex} −4.86/5.45% (10 wt%):η_c −9.58/10.02 cd A^{-1}; η_p −7.8/8.25 lm W^{-1}; η_{ex} −5.96/6.25% (20 wt%). The doped device based on TAPC host TAPC:DDPPPA/TAPC:DDPBA exhibits maximum efficiencies of η_c −9.60/10.03 cd A^{-1}; η_p −7.81/8.26 lm W^{-1}; η_{ex} −5.96/6.25% (20 wt%).

1. Introduction

Efficient deep blue emitters are very important in flat-panel displays because of reduced power consumption[1–3] and to sensitize the dopants for white light emission,[4–6] however, development of blue OLEDs lags behind that of green and red counterparts due to the wider energy gap which leads to unbalanced charge injection/transportation results in poor efficiency.[7–11] Phenanthroimidazole (PI) with pyrrole (N1) and pyridine-like (N3) nitrogen atoms exhibits bipolar characteristics, unmodified PI hinders its application as a potential EL material.[12,13] Therefore, efforts have been made to address these issues by substitution at various positions: C2 substitution induced extended conjugation leads to intramolecular charge transfer (ICT),[14–16] however, N1 substitution does not promote significant photophysical change because of perpendicular configuration[17] and hence, PI derivatives have been designed to have bulky moieties at N1 to control intermolecular interaction in the solid state. The bulky side capping could prevent interactions thereby enhancing the formation of amorphous film and exhibit high PLQY. Therefore it is aimed to incorporate bulky side capping, dihydrobenzodioxin at imidazole nitrogen to reduce packing between the molecules which limits emission quenching leading to enhanced quantum efficiency.[18–22] Designing donor–acceptor (D–A) structure is an effective solution for triplet utilization by reducing exchange energy (J) of exciton and increasing rate of reverse intersystem crossing (RISC):[23–26]

$$K_{RISC} = \frac{2\pi}{\hbar}\langle\varphi_T|H_{So}|\varphi_S\rangle^2 \frac{1}{\sqrt{4\pi\lambda k_{bT}}} \exp\left\{-\frac{(\lambda - \Delta E_{ST})^2}{4\lambda K_b T}\right\} \quad (1)$$

where,

$$\Delta E_{ST} = 2J = 2\left\langle \varphi - \varphi_e \left| \frac{1}{r_{h-e}} \right| \varphi_2 \varphi_1 \right\rangle = 2\frac{\left\{\varphi^*_{h(r_h)}\varphi_{e(r_h)}\right\}\left\{\varphi^*_{e(r_e)}\varphi_{h(r_e)}\right\}}{|r_{h-e}|} \geq 0 \quad (2)$$

where, $|r_{h-e}|$ – distance between hole (h^+) and electron (e^-). Large $|r_{h-e}|$ CT excited state afford ΔE_{ST} to ~zero which induce fast RISC for triplet harvesting[27–33] material exhibit high external quantum efficiency (η_{ex}). Absolute CT excited state materials show poor photoluminescent efficiency (η_{PL}) since large charge

Department of Chemistry, Material Science Lab, Annamalai University, Annamalai Nagar, Tamilnadu-608 002, India. E-mail: jtchalam2005@yahoo.co.in

† Electronic supplementary information (ESI) available. See DOI: 10.1039/d0ra00658k

separation $|r_{h-e}|$ results minimised overlap between hole and electron moieties $\left(\left\langle \varphi_h \middle| \vec{er_\alpha} \middle| \varphi_e \right\rangle\right)$ which leads to decreasing oscillator strength (f) of emissive excited state:

$$f = \frac{2m}{3\hbar^2}(v_e - v_h)\sum_f \sum_{\alpha=x,y,z} \left\langle \varphi_h \middle| \vec{er_\alpha} \middle| \varphi_e \right\rangle^2. \quad (3)$$

Therefore, it is important to construct a material to show high PLQY and exciton utilisation efficiency (η_s) in one excited state. D–A compounds with HLCT (hot exciton model) emissive state show high-exciton utilization efficiency.[34–40] Mixing of LE and CT states are possible when LE as well as CT states are closure in energy, $\Psi(S_1) = \Psi(LE) + \lambda \times \Psi(CT)$; $\lambda = |\langle \Psi_{LE}|H|\Psi_{CT}\rangle / E_{CT} - E_{LE}$. The low-lying higher % LE state provides high radiative rate (k_r) leads to high photoluminescence efficiency (η_{PL}) whereas low-lying higher % CT state provides high η_s through reverse intersystem crossing (RISC) with hot exciton model.[41] The larger energy gap between T_2 and T_1 states reduced internal conversion (IC) ($T_2 \xrightarrow{k_{IC}} T_1$) results hot RISC ($T_2 \xrightarrow{k_{RISC}} S_1/S_2$) than cold RISC ($T_1 \xrightarrow{k_{RISC}} S_1$):[42] hot exciton with HLCT increases η_{EQE} due to coexistence of high η_{PL} and high η_s. The η_{EQE} and η_s can be calculated by, $\eta_{EQE} = \eta_{out} \times \eta_{IQE} = \eta_{out} \times \eta_{rec} \times \eta_\gamma \times \Phi_{PL}$; $\eta_s = \eta_{out} \times \eta_{rec} \times \eta_{PL}$,[43,44], [$\eta_{out}$ – light out-coupling efficiency (20%), η_{rec} – product of the charge recombination efficiency (100%), η_γ – efficiency of radiative exciton production (25%) and Φ_{PL} – photoluminescence quantum yield].

To date, numerous reports have been published on phenanthroimidazole with C2 and N1 substitution, however, substitution at C6 and C9 positions have not been widely studied.[45] Herein, we have designed and synthesized phenanthroimidazole with pyrene substituent at C6 and C9 positions which provides moderate conjugation compared to C2 modification. Photophysical study demonstrates that character transfer of DDPPPA and DDPBA increase as increasing the bulkiness of C6 and C9 substituent. The blue device with DDPBA emissive layer show sky blue emission (470 nm, CIE-0.15, 0.10) with maximum efficiencies: η_c −12.0 cd A^{-1}; η_p −9.2 lm W^{-1}; η_{ex} −6.0% at 2.2 V. The doped device *m*-MTDATA:DDPPPA/*m*-MTDATA:DDPBA show maximum efficiencies of η_c −7.4/8.23 cd A^{-1}; η_p −5.8/6.13 lm W^{-1}; η_{ex} −4.72/5.63% (5 wt%):η_c −8.36/9.15 cd A^{-1}; η_p −6.32/6.65 lm W^{-1}; η_{ex} −4.86/5.45% (10 wt%):η_c −9.58/10.02 cd A^{-1}; η_p −7.8/8.25 lm W^{-1}; η_{ex} −5.96/6.25% (20 wt%). The doped device based on TAPC host TAPC:DDPPPA/TAPC:DDPBA exhibit maximum efficiencies of η_c −9.60/10.03 cd A^{-1}; η_p −7.81/8.26 lm W^{-1}; η_{ex} −5.96/6.25% (20 wt%).

2. Experimental section

2.1. Measurements

^{1}H and ^{13}C NMR measurements were recorded on Bruker 400 MHz spectrometer using TMS as internal standard and mass spectra was recorded on Agilent LCMS VL SD. The UV-optical spectra were measured on Lambda 35 PerkinElmer (solution)/Lambda 35 spectrophotometer (RSA-PE-20) (film). The emission spectra were recorded with PerkinElmer LS55 spectrometer. The quantum yield was measured with fluorescence spectrometer Model-F7100 with integrating sphere. The decomposition temperature (T_d) and T_g (glass transition temperature) was measured with PerkinElmer thermal analysis system (10 °C min^{-1}; N_2 flow rate – 100 ml min^{-1}) and NETZSCH (DSC-204) (10 °C min^{-1}; N_2 atmosphere), respectively. Fluorescence lifetime was estimated by time correlated single-photon counting (TCSPC) method on Horiba Fluorocube-01-NL lifetime system: nano LED is excitation source with TBX-PS is detector; DAS6 software was employed to analyze the decay by reconvolution method. Oxidation potential of emissive materials was measured from potentiostat electrochemical analyzer (CHI 630A). Ferrocene was used as internal standard with HOMO of −4.80 eV and 0.1 M tetrabutylammoniumperchlorate in CH_2Cl_2 as supporting electrolyte.

2.2. Synthesis of materials

2.2.1. 4-(6,9-Dibromo-1-(2,3-dihydrobenzo[*b*][1,4]dioxin-5-yl)-1*H*-phenanthro[9,10-*d*]imidazol-2-yl)-*N*,*N*-diphenylaniline (DPPB). A mixture of 3,6-dibromophenanthrene-9,10-dione (3 g, 8.2 mmol), 4-(diphenylamino)benzaldehyde (3.38 g, 12.3 mmol), 1,4-benzodioxane-6-amine (4.65 g, 50 mmol) and ammonium acetate (7.85 g, 101.8 mmol) in glacial acetic acid (40 ml) was refluxed for 12 h (N_2 stream). The yellow solution was poured into ethanol and the separated solid was washed with methanol and dried. The solid was purified by column chromatography (hexane : ethylacetate) yield: 66%. ^{1}H NMR (400 MHz, $CDCl_3$): 4.36 (s, 4H), 6.46–6.52 (m, 6H), 6.62–6.7 (m, 5H), 7.01 (q, 2H), 7.23 (d, 2H), 7.71 (s, 4H), 7.82–7.93 (m, 10H), 8.04–8.18 (m, 8H), 9.15 (s, 2H). ^{13}C NMR ($CDCl_3$, 100 MHz): 64.3, 114.5, 114.6, 118.1, 122.0, 122.3, 122.7, 124.0, 124.9, 125.1, 126.0, 126.3, 126.6, 128.0, 128.3, 128.4, 129.7, 132.0, 133.3, 133.4, 137.0, 137.7, 141.0, 147.6, 149.4. MS: *m*/*z*. 753.06 [M^+]; calcd 753.04.

2.2.2 4-(1-(2,3-Dihydrobenzo[*b*][1,4]dioxin-5-yl)-6,9-di(pyren-4-yl)-1*H*-phenanthro[9,10-*d*]imidazol-2-yl)-*N*,*N*-diphenylaniline (DDPPPA). A mixture of DPPB (1.5 g, 2 mmol), pyren-1-yl-1-boronic acid (0.97 g, 4.4 mmol), $Pd(PPh_3)_4$ (0.26 g, 0.40 mmol) and aqueous Na_2CO_3 (2 M, 8 ml) in toluene (30 ml) and ethanol (6 ml) was refluxed (36 h; N_2 stream). The solution was cooled to room temperature and extracted with dichloromethane. The residue was purified by column chromatography (hexane : ethylacetate) to obtain light yellow powder. Yield: 69%. ^{1}H NMR (400 MHz, $CDCl_3$): 4.36 (s, 4H), 6.52–6.46 (m, 6H), 6.62–6.7 (m, 5H), 7.01 (t, 4H), 7.23 (d, 2H), 7.71 (d, 2H), 7.82–7.93 (m, 10H), 8.04–8.18 (m, 8H), 9.15 (d, 2H). ^{13}C NMR ($CDCl_3$, 100 MHz): 64.3, 114.5, 114.6, 118.1, 121.9, 122.0, 122.3, 122.7, 123.2, 124.9, 125.1, 125.4, 125.7, 126.3, 126.5, 126.6, 128.3, 128.4, 129.7, 132.0, 133.4, 134.3, 137.0, 137.7, 141.0, 147.6, 149.4. MS: *m*/*z*. 996.16 [M^+]; calcd 996.19.

2.2.3. 4′-(6,9-Dibromo-1-(2,3-dihydrobenzo[*b*][1,4]dioxin-5-yl)-1*H*-phenanthro[9,10-*d*]imidazol-2-yl)-*N*,*N*-diphenyl-[1,1′-biphenyl]-4-amine (DPDA). A mixture of 3,6-dibromophenanthrene-9,10-dione (3 g, 8.2 mmol), 4′-(diphenylamino)-[1,1′-biphenyl]-4-carbaldehyde (3.38 g, 12.3 mmol), 1,4-benzodioxane-6-amine

(4.65 g, 50 mmol) and ammonium acetate (7.85 g, 101.8 mmol) in glacial acetic acid (40 ml) was refluxed (12 h; N_2 stream). The yellow coloured solution was poured into ethanol and the solid was purified by column chromatography (hexane : ethylacetate) yield: 52%. ^{1}H NMR (400 MHz, $CDCl_3$, ppm): 4.36 (s, 4H), 6.46–6.52 (m, 6H), 6.62–6.7 (m, 5H), 7.01 (q, 4H), 7.23 (d, 2H), 7.71 (s, 4H), 7.82–7.93 (m, 10H), 8.04–8.18 (m, 8H), 9.15 (s, 2H). ^{13}C NMR ($CDCl_3$, 100 MHz): 64.3, 114.5, 114.6, 118.1, 122.0, 122.3, 122.7, 124.0, 124.9, 125.1, 126.0, 126.3, 126.6, 128.0, 128.3, 128.4, 129.7, 132.0, 133.3, 133.4, 137.0, 137.7, 141.0, 147.6, 149.4. MS: *m*/*z*. 995.38 [M]$^+$; calcd: 995.35. Anal. calcd (%) for $C_{73}H_{45}N_3O_4$: C, 88.02; H, 4.55; N, 4.22. Found: C, 87.97; H, 4.60; N, 4.18.

2.2.4. 4′-(1-(2,3-Dihydrobenzo[*b*][1,4]dioxin-5-yl)-6,9-di(pyren-4-yl)-1*H*-henanthro[9,10-*d*]imidazol-2-yl)-*N*,*N*-diphenyl-[1,1′-biphenyl]-4-amine (DDPBA). A mixture of DPDA (1.5 g, 2 mmol), pyren-1-yl-1-boronic acid (0.97 g, 4.4 mmol), $Pd(PPh_3)_4$ (0.26 g, 0.40 mmol) and aqueous Na_2CO_3 (2 M, 8 ml) in a mixture of toluene (30 ml) and ethanol (6 ml) was refluxed (36 h; N_2 stream). The solution was extracted with dichloromethane and the residue was purified by column chromatography (hexane : ethylacetate) yield: 69%. ^{1}H NMR (400 MHz, $CDCl_3$): 4.36 (s, 4H), 6.46–6.52 (m, 6H), 6.62–6.7 (m, 5H), 7.01 (q, 4H), 7.23 (d, 2H), 7.54 (s, 4H), 7.71 (d, 4H), 7.82–7.93 (m, 10H), 8.04–8.18 (m, 8H), 9.15 (d, 2H). ^{13}C NMR ($CDCl_3$, 100 MHz): 64.3, 114.5, 114.6, 118.1, 121.9, 122.0, 122.7, 123.2, 124.9, 125.2, 125.4, 126.3, 126.5, 128.0, 128.3, 128.4, 128.8, 129.6, 129.7, 130.9, 132.0, 133.2, 133.3, 134.4, 136.5, 137.7, 139.9, 141.0, 147.6, 149.4. MS: *m*/*z*. 1071.44 [M$^+$]; calcd 1071.38.

2.3. Device fabrication and measurement

ITO glass (resistance 20 Ω sq^{-1}) were cleaned with acetone, deionized water and isopropanol, dried (120 °C) followed by UV–ozone treatment (20 min) and transferred into deposition system. The devices were fabricated by the multiple source beam deposition method in a vacuum at a pressure of 4×10^{-5} mbar. Evaporation rates of 2–4 Å s^{-1} (organic materials) and 0.1 and 4 Å s^{-1} for LiF and metal electrodes were applied, respectively. The thickness of each deposition layer was monitored with quartz crystal thickness monitor. The EL measurement with CIE coordinates was recorded with USB-650-VIS-NIR spectrometer (Ocean Optics, Inc, USA). The current density–voltage–luminance (*J*–*V*–*L*) characteristics was performed using source meter (Keithley 2450) equipped with LS-110 light intensity meter. The η_{ex} (external quantum efficiency) was determined from luminance, current density and EL spectrum assuming Lambertian distribution.

2.4. Computational details

The ground (S_0) (DFT)/excited (S_n^*) (TD-DFT) states of emissive materials were analyzed by Gaussian 09 program[46] and multifunctional wavefunction analyzer (Multiwfn).[46] The natural transition orbitals (HONTOs & LUNTOs) with hole-particle contribution were studied in detail. The TDM (transition density matrix) map of emissive materials was analyzed to support HLCT character.

3. Results and discussion

The synthetic route for the emissive materials is displayed in Scheme S1:† efficient blue emitters namely, 4-(1-(2,3-dihydrobenzo[*b*][1,4]dioxin-5-yl)-6,9-di(pyren-4-yl)-1*H*-phenanthro[9,10-*d*]imidazol-2-yl)-*N*,*N*-diphenylaniline (DDPPPA) and 4′-(1-(2,3-dihydrobenzo[*b*][1,4]dioxin-5-yl)-6,9-di(pyren-4-yl)-1*H*-phenanthro[9,10-*d*]imidazol-2-yl)-*N*,*N*-diphenyl-[1,1′-biphenyl]-4-amine (DDPBA) were synthesized by Suzuki-coupling reaction with appreciable yield and characterized by spectral techniques.

3.1. Thermal and electrochemical properties

The twisting angle between pyrene and phenanthroimidazole plane of D–π–A structured DDPPPA and DDPBA is about ∼55° which effectively suppress the conjugation and intermolecular π–π stacking. The twisted molecular architecture has been increased the thermal stability of DDPPPA and DDPBA and the excellent thermal stability was analyzed by high decomposition temperature (T_d, 5% weight loss). The high T_d (556 °C-DDPPPA; 562 °C-DDPBA) reveals that these compounds would be capable of enduring vacuum thermal sublimation process. Both compounds show high glass transition temperature (T_g: 201 °C-DDPPPA; 223 °C-DDPBA) indicating that pyrene substituent at C6 and C9 positions and bulky substituent at N-side coupling of rigid phenanthroimidazole enhanced their morphological stability (Table 1 and Fig. 1). The interaction of substituent at C2- and N1 of phenanthroimidazole core improved T_g and induced more condensed molecular packing. The higher T_g reveal that morphologically stable amorphous film will form on thermal evaporation which reduced the phase separation on heating and improving the lifetime of devices. The thermal morphological stability of thin film of these compounds was examined by atomic-force microscopy at 30 °C and 90 °C for 12 h. The root-mean-square (0.24 nm-DDPPPA; 0.28 nm-DDPBA) reveal absence of remarkable surface modification before and after annealing which further supports the suitability of these materials for fabrication.

The DDPPPA and DDPBA shows quasi-reversible oxidation and reduction process with an oxidation onset potential (E_{onset}) of 0.82 (DDPPPA) and 0.80 V (DDPBA), implying that these materials are electrochemically stable and are bipolar carrier-transporting materials.[47] The E_{HOMO}[−(E_{onset} + 4.8 −

Table 1 Optical and thermal properties of DDPPPA and DDPBA

Characteristics	DDPPPA	DDPBA
λ_{ab} (nm) (sol)	248, 275, 342	240, 268, 334
λ_{em} (nm) (sol/film)	480/456	469/448
T_g/T_d (°C)	201/556	223/562
ϕ (soln/film)	96/83	98/85
HOMO/LUMO (eV)	−5.22/−2.39	−5.20/−2.41
E_g (eV)	−2.83	−2.79
τ (ns)	1.38	1.13
$k_r \times 10^8$ (s^{-1})	0.69	0.03
$k_{nr} \times 10^8$ (s^{-1})	0.87	0.01

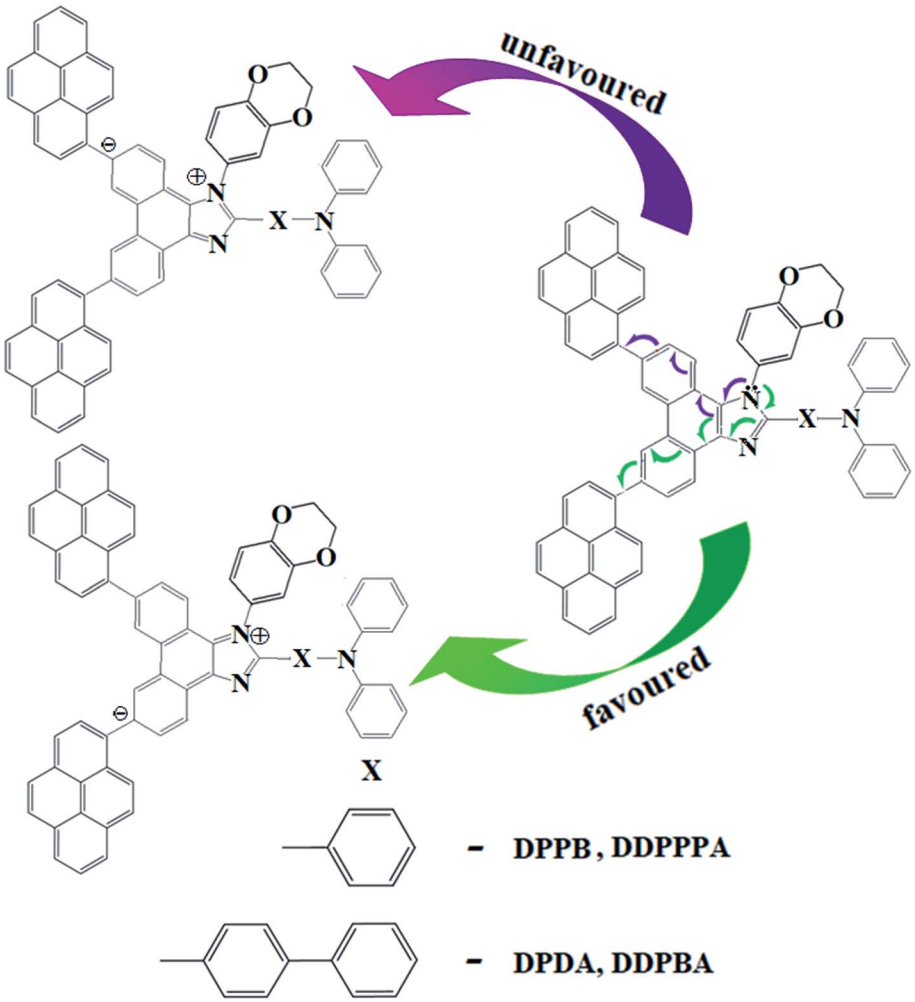

Fig. 1 Favoured and unfavoured configurations of blue emitters.

$E_{ferrocene}$)] eV and $E_{LUMO}[E_{HOMO} - 1239/\lambda_{onset}]$ have been calculated as DDPPPA (HOMO −5.22 eV; LUMO −2.39 eV) and DDPBA (HOMO −5.20 eV; LUMO −2.41 eV).

3.2. Photophysical properties

The absorption and emission of DDPPPA and DDPBA was studied with various solvents and also in film (Fig. 1). The strong absorption around 236 nm can be attributed to π–π* transition of phenyl ring attached to N-atom in imidazole ring.[48] The absorption around 268 nm can be ascribed to absorption of diphenylamine unit.[49] The extinction coefficient (ε_{max}) of D–π–A molecules is due to increase of conjugation length:[50,51] DDPPPA and DDPBA show very strong absorption at 240 nm (ε_{max} = 41 666 cm^{-1} M^{-1}) and 236 nm (ε_{max} = 42 372 cm^{-1} M^{-1}) due to ICT transition from donor to acceptor (Fig. 2). The film state of blue emissive materials show absorption at 244 nm (DDPPPA) and 240 nm (DDPBA) and the small shift shows the existence of weak π–π* intermolecular stacking.[52] The shoulder peak at longer wavelength around 334 nm might be attributed to an intramolecular charge transfer (ICT) from electron donating diphenylamine to electron-withdrawing imidazole unit.[53] The solution/film PL spectra of DDPPPA and DDPBA show emission maxima at 480/456 and 469/448 nm, respectively (Fig. 2). These compounds DDPPPA and DDPBA show shorter wavelength emission relative to C2-substituted compounds. Overall, substitution at C6 and C9 positions of phenanthroimidazole ring in DDPPPA and DDPBA induces moderate π-conjugated extension comparing to C2-modified ones.

The solvatochromic effect using Lippert–Mataga plot has been displayed in Fig. 2. When solvent polarity increased the blue emitters exhibit a larger red shift which supports the charge transfer in these molecules. The emission spectra gradually broadened with large red shift of 30 nm (DDPPPA) and 65 nm (DDPBA) reveal that their excited state possess strong CT characteristics (Fig. S1†).[54] The red shifted emission is due to twisted conformation of DDPPPA and DDPBA which leads to easier charge transfer from donor to accept *via* aryl linker. The intramolecular charge transfer is further confirmed by molecular electrostatic potential (MEP) (Fig. 2).[55,56] Interaction between solvent and dipole moment of solute can be described by the Lippert–Mataga model.[57] $hc(\tilde{\nu}_{abs} - \tilde{\nu}_{flu}) = hc(hc\Delta_{abs}^{vac} - hc\Delta_{flu}^{vac}) + 2(\mu_e - \mu_g)^2/a_o{}^3[(\varepsilon - 1/2\varepsilon + 1) - \frac{1}{2}(n^2 - 1/2n^2$

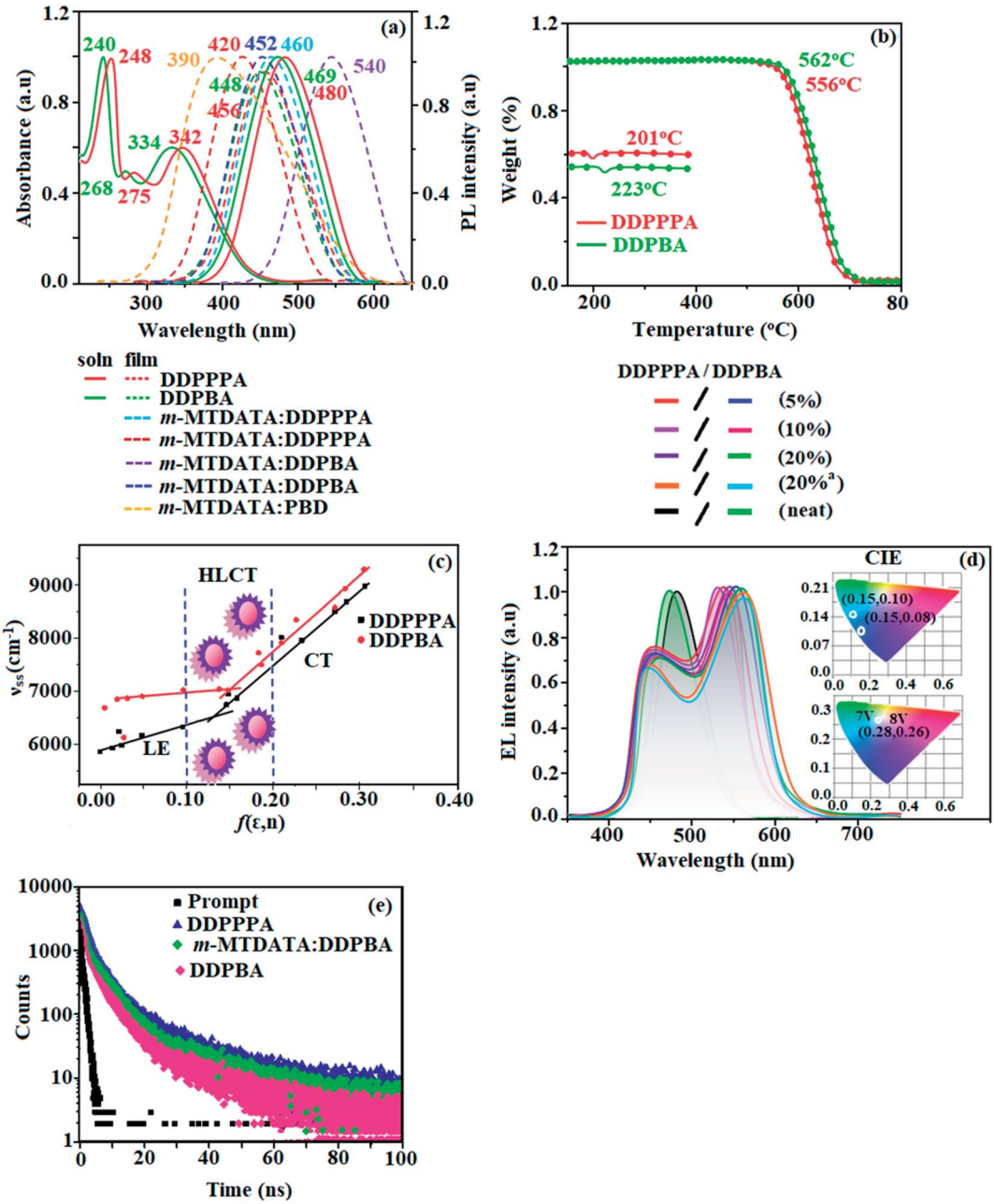

Fig. 2 (a) Normalized absorption and emission spectra; (b) TGA and DSC; (c) Lippert–Mataga plot; (d) decay curve; (e) EL spectra (inset: CIE coordinates) of DDPPPA and DDPBA.

+ 1)] [μ_g and μ_e – ground state and excited state dipole moment, $\tilde{\nu}_{abs}$ and Δ_{abs}^{vac} – solvent-equilibrated absorption maxima (λ_{abs}) and extrapolated to gas phase, $\tilde{\nu}_{flu}$ and Δ_{flu}^{vac} – solvent equilibrated fluorescence maxima (λ_{emi}) and extrapolated to gas-phase, respectively, a_o – onsager cavity and ε and n – solvent dielectric constant and refractive index, respectively].

The ground state dipole moment (μ_g) of blue emitting materials, DDPPPA and DDPBA could be estimated from DFT calculation as 8.67 and 7.45 D, respectively which is attributed by local exciton (LE) transition. From Lippert–Mataga plot (Fig. 2, Table S1 – DDPPPA and Table S2 – DDPBA†), the excited state dipole moment (μ_e) in high polar solvents is calculated to be 25.6 and 27.3 D, respectively. A transformation in the slope of the fitted line is observed between ether ($f = 0.10$) and ethyl acetate ($f = 0.20$) solvents. This implies that these blue emitters show HLCT excited state. The fluorescent solvatochromic experiments and non-linear relationship of Stokes shift with solvent polarity indicate that our new born molecules DDPPPA and DDPBA possess intercrossed excited state of LE and CT. The large μ_e in high polar medium is in close with μ_e of charge-transfer molecule, 4-(*N*,*N*-dimethylamino)benzonitrile (23.0 D). All these results show that CT dominates in more polar medium ($f \geq 0.2$) and LE dominates in low polar solvents ($f \leq 0.1$) and there is mixed contribution of LE and CT in medium

polar solvents. The new born blue emitters show high quantum yield (solution/film) of DDPPPA (0.96/0.83) and DDPBA (0.98/0.85) and high fluorescence yield is essential for efficient blue OLEDs (Table 1). It is unique that CT material shows efficient deep-blue emission; the co-emission from LE and CT (intercrossed CT and LE state) is likely to be the reason for high fluorescence yield. The oscillator strength (f) for $\lambda_{abs}/\lambda_{emi}$ of DDPPPA (gas phase – 372 (f – 1.5283)/383 (f – 1.7692); $CHCl_3$ – 368 (f – 1.7982)/412 (f – 2.0462)) and DDPBA [gas phase – 380 (f – 1.5846)/392 (f – 1.8146); $CHCl_3$ – 370 (f – 1.8268)/422 (f – 1.9432)] reveal that oscillator strength of these compounds in $CHCl_3$ is high when compared to gas phase which reveal the higher luminescence of intercrossed excited state in $CHCl_3$.

3.3. Theoretical calculation

To gain a better insight into the electronic structure of DDPPPA and DDPBA, DFT calculations were carried out at B3LYP/6-31G (d) level. As shown in (Fig. 3), in DDPPPA and DDPBA, HOMO orbital was partially extends to pyrene plane whereas due to stronger electron withdrawing ability of pyrene, phenanthroimidazole unit makes much less contribution to LUMO. The LUMO orbital localized on C9-pyrene with less contribution from C6 pyrene and this asymmetry originates from the difference in LUMO contribution of C6 and C9. In C4 and C7-modified benzimidazole asymmetry compounds having different reactivity difference at C4 and C7 brominated sites in Suzuki coupling reaction due to two different nitrogen atoms in imidazole ring,[57] thus, similar properties can be expected in phenanthroimidazole: obey Huckel's ($4n + 2$) rule (Fig. 3). The lone pair electrons at N1 involved in the formation of conjugated system whereas the lone pair on N3 has no contribution. The conjugated lone pair electrons can be transferred toward C6 or C9: electron migration toward C6 is more favourable since it results in largest charge-separated distance than C9 (green arrow) (Fig. 3). This preferred electronic structure leads to charge accumulation at C6 position. This unique electronic structure induced the electron delocalisation on HOMO and LUMO of DDPPPA and DDPBA at C6 and C9 substitutions, respectively and hence, this asymmetry enhanced the electron injection, however, there is small overlap in HOMO and LUMO orbitals. This is more likely to endow DDPPPA and DDPBA with bipolar charge transporting ability become more efficient emitters in OLEDs.[58] The HONTOs and LUNTOs of DDPPPA (Fig. S2 and Table S3†) and DDPBA (Fig. S3 and Table S4†) exhibit a hybrid splitting state character from interstate coupling of LE and CT levels (Tables S5 and S6 – DDPPPA and Tables S7 and S8 – DDPBA†). The hole contour on TPA is in the opposite phases between S_1 and S_2 states whereas the particle contour on phenanthroimidazole moiety is same between S_1 and S_2 states for DDPPPA and DDPBA. This reveal that the interstate hybridization coupling between LE and CT state wave function: $\Psi_{S_1/S_2} = c_{LE}\Psi_{LE} \pm c_{CT}\Psi_{CT}$. The % CT of DDPPPA and DDPBA increases as increasing the aromatic fragment size and also partially influenced by steric hindrance. As increasing % LE in S_1 state of DDPPPA (LE $\sim$ 30%) and DDPBA (LE $\sim$ 40%) these emitters exhibit higher photoluminescence efficiency (η_{PL}). The formation of single emissive state can be analyzed through excitation energies of LE and CT states. A large energy gap between T_1 and T_2 of DDPPPA (0.75 eV) and DDPBA (1.07 eV) arising from the same phenanthroimidazole acceptor group and the energy gap between T_1 and T_2 of DDPBA is larger than

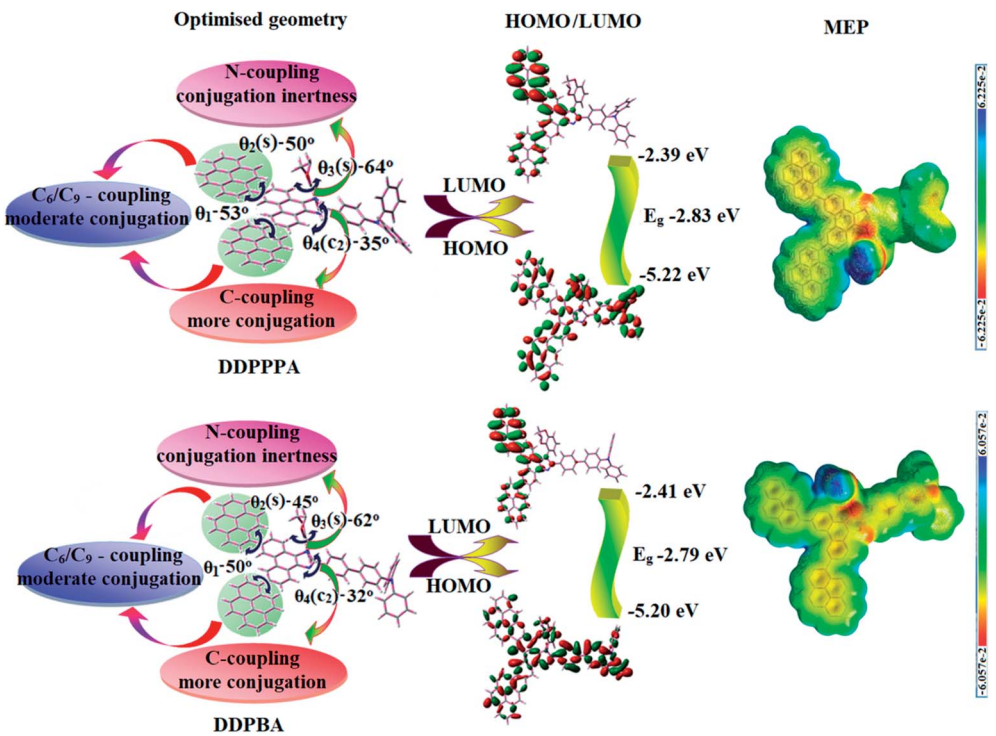

Fig. 3 Optimised geometry with dihedral angles, HOMO–LUMO map and MEP of DDPPPA and DDPBA.

DDPPPA (Fig. S4†).[59,60] A very small $\Delta E_{ST} \approx 0$ between S_1 and T_2 states facilitating RISC ($T_2 \rightarrow S_1$) process in both DDPPPA (Tables S9 and S10†) and DDPBA (Tables S11 and S12†) as a result of HLCT character (Fig. S5†). Thus, compared with DDPPPA, DDPBA exhibits high photoluminescence efficiency (η_{PL}), high exciton utilisation efficiency (η_s) and high external quantum efficiency (η_{EQE}) as a result of increased LE component in S_1 state.

Similar hole–electron wave function between S_1 and S_2 in both DDPPPA and DDPBA indicates quasi-equivalent hybridization between LE and CT states due to isoenergies of initial LE and CT states (Fig. S5†). Therefore, degree of hybridization between LE and CT states depend not only initial E_{LE}–E_{CT} energy gap but also their interstate coupling strength.[61] Compared with non-equivalent hybridization, quasi-equivalent hybridization leads to high η_{PL} and high η_s to maximize EL efficiency of fluorescent OLED materials due to more balanced LE and CT components in HLCT state of DDPPPA and DDPBA. In DDPPPA and DDPBA, the LE state is stabilized than CT state and energy gap (E_{S_2}–E_{S_1}) is small when compared with their parent compounds results effective quasi hybridization (Fig. S5†) and improves OLED efficiency. Composition of HLCT can be discussed from wave function of electron–hole pairs transition density matrix (TDM) and plot them in two-dimension colour-filled map (Fig. S6 – DDPPPA and Fig. S7 – DDPBA†). The diagonal region represents LE component and off-diagonal region shows CT component. Upon excitation, electron is transferred from donor and localized on acceptor: depending upon intramolecular geometrical and electronic coupling, transferred electron is delocalized from the region of nearby donor to the vicinity of acceptor. This effect can be qualitatively studied by analyzing electron density distribution at ground and excited states. Computed electron–hole properties, distance between hole and electron, transition density, *H* and *t* indexes and RMSD of electron and hole of DDPPPA and DDPBA are displayed in Tables S9–S12,† respectively.

The integral value of hole and electron of DDPPPA (Table S5†) is higher than DDPBA (Table S6†) with transition density. The integral overlap of hole–electron distribution (*S*) is a measure of spatial separation of hole and electron. The integral overlap (*S*) of hole and electron and distance (*D*) between centroids of hole and electron evidences the existence of LE and CT states (Tables S5 and S7†). The emitters DDPPPA and DDPBA show small *D* and high *S*, however, small *D* and high *S* of DDPPPA on comparison with DDPBA indicates higher charge transfer (CT) for DDPPPA. The variation of dipole moment with respect to S_0 state is outputted which is directly evaluated based on the position of centroid of hole and electron. RMSD of hole or electron characterizes their distribution breadth: RMSD of both electron and hole in DDPPPA (Tables S9 and S10†) and DDPBA (Tables S11 and S12†) is higher in *Z* direction indicates electron and hole distribution is much broader in *Z* direction whereas RMSD of electron and hole of DDPPPA is higher than DDPBA. The overlap between the region of density depletion and increment have been visualised by using two centroids of charges (eqn (S9) and (S10)†). Using this arbitrarily condensed function, computed overlap of ρ_+ and ρ_- regions for DDPPPA and DDPBA is 0.9843 and 0.9985, respectively (Table S13†). Similarly, *H* index of DDPPPA is higher than DDPBA. The CT index, *i.e.*, *t* index difference between D_{CT} and *H* index is another measure of the separation of hole–electron (eqn (S15) and (S16)†); *t* index of DDPPPA is higher than DDPBA. The D_{CT}/μ_{CT} of DDPPPA and DDPBA was calculated to be 1.201/0.003 and 0.429/59.23, respectively (Fig. S8 and Table S13†). For both DDPPPA and DDPBA, the non-zero *t* is negative in all directions: overlap of hole and electron is very severe (Fig. S8†) and eign value is greater than 0.94, supports the hybridization with dominant excitation pair in term of 92% of transition.

The hybridization and HLCT is further evidenced by Δr index (Table S14 – DDPPPA and Table S15 – DDPBA†). The Δr index (eqn (S1)†) is average of hole (h^+)–electron (e^-) distance ($d_{h^+-e^-}$) upon excitation which implies the nature of the excitation type, LE or CT: valence excitation (LE) is related to short distances ($d_{h^+-e^-}$) while larger distances ($d_{h^+-e^-}$) related to CT excitation. The triplet exciton is transformed to singlet exciton in DDPPPA and DDPBA *via* RISC process with high energy excited state (hot CT channel)[62] which is beneficial for triplet exciton conversion in electroluminescence process without delayed fluorescence (Fig. S4†). The CT excitons are formed with weak binding energy (E_b) on higher excited states.[63] As a result, the exciton utilization (η_s) can be harvested in DDPPPA and DDPBA like phosphorescent materials. The quasi-equivalent hybridized materials DDPPPA and DDPBA show excellent device performances due to fine modulation in excited states: enhanced LE component and hybridization between LE and CT components results high η_{PL} and high η_s and enhanced OLEDs performances (Table 2). These compounds exhibit blue emission with high quantum yield (solution/film) of DDPPPA (0.96/0.83) and DDPBA (0.98/0.85) and high fluorescence efficiencies are essential for efficient blue OLEDs. The ΔE_{ST} of these hosts are relatively small which arises from spatially separated HOMO and LUMO of those hosts. The small ΔE_{ST} are advantageous for efficient energy transfer from triplet excited state of hosts to green and red phosphorescent emitters.[64]

The potential energy surfaces (PES) have been plotted as a function of twist angle between C2 substituent and phenanthroimidazole core in gas phase and different polarity solvents (Fig. S9†). In gas phase, it is impossible for S_3 mixing with S_1 state as a result of large energy gap between them. An increasing solvent polarity, the large dipole moment of S_3 state leads to a significant energetic stabilization. In low polarity solvent (hexane), S_3 state can intercross with S_1 state whereas in high polarity solvent (acetonitrile), S_3 state energy decreases sharply and becomes lowest excited state. In moderate polar solvents (chloroform), the energetic closeness results in an enhanced mixing of S_3 with S_1. Therefore, in low polarity, S_1 state is dominated by LE character; in moderate polarity, S_1 state is dominated by mixing LE and CT character; in high polarity, S_1 state is dominated by CT character.

3.4. Electroluminescent properties

To understand the carrier transport abilities of DDPPPA or DDPBA, hole-only and electron-only devices have been fabricated with configuration of ITO/NPB (8 nm)/DDPPPA or DDPBA

Table 2 Comparative non-doped and doped device efficiencies

Emitters	Concentration	V_{on} (V)	L (cd m^{-2})	EL (nm)	η_c (cd A^{-1})	η_p (lm W^{-1})	η_{ex} (%)	η_{IQE} (%)	η_s (%)	CIE (x, y)
DDPPPA	5%	4.6	8123	448, 536	7.40	5.8	4.72	23	25.8	0.28, 0.28
	10%	4.2	9082	448, 535	8.36	6.32	4.86	24	26.9	0.28, 0.27
	20%	3.8	11 260	448, 537	9.58	7.80	5.96	29	32.5	0.28, 0.26
	20%[a]	3.8	11 265	448, 540	9.60	7.81	5.96	29	32.5	0.28, 0.26
	Non-doped	2.3	10 582	480	10.50	8.30	5.70	28	31.4	0.15, 0.08
DDPBA	5%	4.5	10 462	488, 538	8.23	6.13	5.63	28	31.1	0.28, 0.28
	10%	4.0	11 862	488, 537	9.15	6.65	5.45	27	30.0	0.28, 0.27
	20%	3.2	14 021	448, 539	10.02	8.25	6.25	31	34.4	0.28, 0.26
	20%[a]	3.2	13 897	447, 540	10.03	8.26	6.25	31	34.4	0.28, 0.26
	Non-doped	2.2	12 634	470	12.00	9.20	6.00	30	33.3	0.15, 0.10

[a] ITO/NPB (40 nm)/TAPC:DDPPPA or TAPC:DDPBA (20 nm)/TPBi(25 nm)/LiF (1 nm)/Al (100 nm).

(40 nm)/NPB (8 nm)/Al (100 nm) (hole-only device): NPB (LUMO: −2.3 eV) in the hole-only device can prevent electron injection from Al cathode (E_f – 4.3 eV)[65] and ITO/TPBi (8 nm)/DDPPPA or DDPBA (40 nm)/TPBi (8 nm)/LiF (1 nm)/Al (100 nm) (electron-only device): TPBi (HOMO: −6.2 eV) in the electron-only device with ITO (E_f – 4.8 eV) as the anode can prevent hole injection.[66] The current density *versus* voltage characteristics of hole-only and electron-only devices was displayed in Fig. 4. The hole-only and electron-only devices show the same current density values at same voltage indicating that these compounds are bipolar materials. The electron current density of DDPPPA or DDPBA based device is higher than CBP-based device (Fig. 4) which reveals that these compounds are bipolar-transporting materials with effectively transporting electrons and or holes than CBP.[67–69]

Two non-doped OLEDs were fabricated: ITO/NPB (70 nm)/TCTA (5 nm)/DDPPPA and DDPBA (30 nm)/TPBI (40 nm)/LiF (1 nm)/Al (150 nm) NPB – hole-transporting layer (HTL), TPBI – electron transporting layer (ETL) as well as hole blocking layer, DDPPPA and DDPBA – emitting layer (EML) and ITO and LiF/Al are used as anode and cathode, respectively (Fig. 5). Because of high HOMO energies of DDPPPA (−5.22 eV) and DDPBA (−5.20 eV) there is negligible hole injection barrier at TCTA:EML interface [DDPPPA (−0.48 eV) and DDPBA (−0.50 eV)]. Similarly, electron-injection barrier at TPBI:EML interface also small [DDPPPA (−0.31 eV) and DDPBA (−0.29 eV)], hence, small injection barrier promotes efficient hole and electron injection as well as transportation into the emission layer.[70] Therefore, devices based on DDPPPA and DDPBA show maximum efficiency at low turn-on voltages of 2.3 and 2.2 V, respectively (Fig. 4). Electroluminescence (EL) spectra of DDPPPA (480 nm) and DDPBA (470 nm) show sky-blue emission with CIE (0.15, 0.08) and (0.15, 0.10), respectively (Fig. 1). Their EL spectra are almost same as that of PL spectra of the corresponding film. Absences of other peaks reveal that carrier recombination is well confined within the emissive layer.[71]

The non-doped device with DDPPPA/DDPBA shows maximum η_c, η_p and η_{ex} of 10.5/12 cd A^{-1}, 8.3/9.2 lm W^{-1} and 5.7/6.0%, respectively (Fig. 4). The maximum exciton-utilizing efficiency (η_s) of the devices based on DDPPPA/DDPBA calculated as 31.4 and 35.3%, respectively, exceeds 25% theoretical limit of spin statistics for conventional fluorescent OLEDs. This can be attributed to the effective utilization of both energies of LE and CT exciton (*i.e.*, hybridized local and charge-transfer). The high η_s is likely to be a result of an exciton channel *via* potential RISC from upper excited states (Fig. S4†).[72] To the best of our knowledge, these efficiencies are highest EL efficiencies with CIEy <0.3 that have been reported[73–83] (Table 3). We also observed that the luminance has a good linear relationship with current density shows that the enhanced η_s is not from triplet–triplet annihilation process. Transient PL decays (Fig. 1) reveal single-exponential lifetime of 1.38 ns (DDPPPA) and 1.13 ns (DDPBA). The single-lifetime decay profiles suggest that the LE and CT states are highly hybridized.[84]

To further improve the efficiency and colour purity, we have used DDPPPA and DDPBA as emissive dopant and 4,4′,4″-tris[3-methylphenyl(phenyl)amino]triphenylamine (*m*-MTDATA) as host to fabricate OLEDs. In this host-guest system, the emissive materials are diluted in the host matrix, not only device efficiency and colour purity is also improved *via* efficient Förster energy transfer. Electroluminescent devices based on doped light-emitting layers with ITO/NPB (40 nm)/*m*-MTDATA:DDPPPA or *m*-MTDATA:DDPBA (20 nm)/TPBi (25 nm)/LiF (1 nm)/Al (100 nm) have been fabricated. Herein, NPB (*N*,*N*′-di-1-naphthyl-*N*,*N*′-diphenylbenzidine) and TPBi functioned as electron- and hole-blocking materials, respectively. 4,4′,4″-tris[3-Methylphenyl(phenyl)amino]triphenylamine (*m*-MTDATA) was employed as hole-transporting as well as electron-blocking layers and 1,3,5-tris(*N*-phenylbenzimidazol-2-yl)benzene (TPBi) was employed as electron-injection layers. These devices show white emission due to the mixed blue monomer emission and orange electroplex emission in the *m*-MTDATA:DDPPPA and or *m*-MTDATA:DDPBA (Fig. 4). The electroluminescence spectra of the doped devices based on DDPPPA/DDPBA (5% – 448, 536/488, 538; 10% – 448, 535/488, 537; 20% – 448, 537/448, 539) is shown in Fig. 2. The low-energy bands were additionally observed in the electroluminescence spectra of the doped OLEDs as compared to non-doped OLEDs EL spectra. Appearance of the additional band can be explained by the formation of dimeric excited states namely, exciplexes and or electroplexes either in doped light-emitting layer or at interface between layers of OLEDs due to cross-interaction between holes of donor

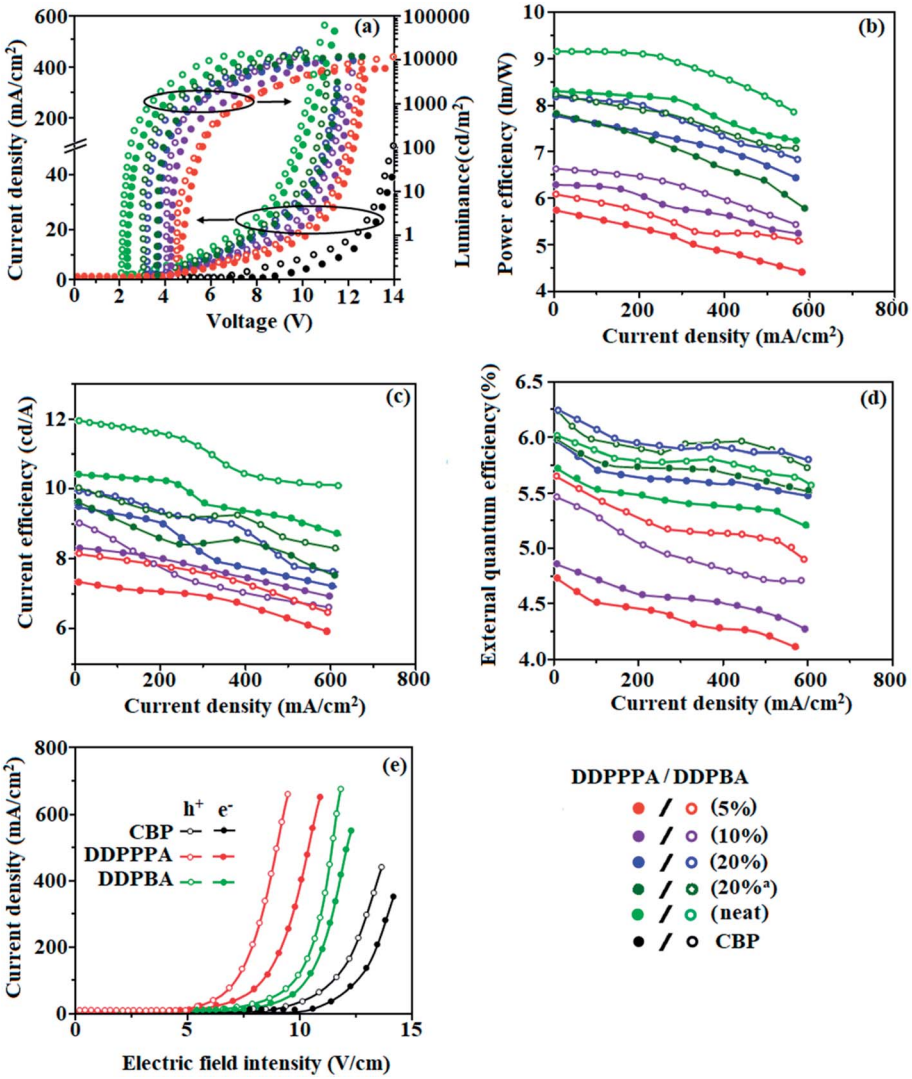

Fig. 4 Device efficiencies: (a) luminance/current density–voltage; (b) power efficiency–current density; (c) current efficiency–current density; (d) external quantum efficiency–current density and (e) current density–electrical field density of DDPPPA and DDPBA.

and electrons of acceptor.[85] To prove this assumption, PL spectra of the film of hosts and emitters molecular mixture were recorded (Fig. 2). The PL spectra of the mixture *m*-MTDATA:DDPPPA and *m*-MTDATA:DDPBA were similar to PL spectra of pure DDPPPA and DDPBA and did not contain bands at wavelength close to low energy band observed in EL spectra of doped OLEDs. The similarity of shapes and positions of the PL spectra of the mixtures to PL spectra of pure emitters (DDPPPA and DDPBA) indicates effective energy transfer from hosts to emitters. However, PL spectra of *m*-MTDATA:PBD is different as compared with PL spectra of pure *m*-MTDATA and PBD, respectively. The maximum at 540 nm of PL spectrum of *m*-MTDATA:PBD film was found to be at similar wavelength as the maximum of additional band in the EL spectra of devices with *m*-MTDATA as the host. The PL decay curve of *m*-MTDATA:PBD show double-exponential function (Fig. 2). The shorter and longer lived components attributed to monomeric fluorescence and exciplex emission, respectively. The exciplex emission is due to reverse intersystem crossing (RISC).[85] Hence, low-energy emission band in EL spectra of doped OLEDs with *m*-MTDATA host can be ascribed to the interface exciplex between *m*-MTDATA and PBD.[85] The CIE of *m*-MTDATA:DDPPPA and *m*-MTDATA:DDPBA and TAPC:DDPPPA and TAPC:DDPBA based device at voltages from 7 V to 8 V was found to be very close to white point (0.28, 0.26) (Fig. 4) due to the mixed blue monomer emission and orange electroplex emission in the *m*-MTDATA:DDPPPA and *m*-MTDATA:DDPBA and TAPC:DDPPPA and TAPC:DDPBA emitting-layer.

Diluting the emitter molecules in the host eliminates the effect of intermolecular close stacking and decreased medium polarity because *m*-MTDATA is generally used as a nonpolar host material.[86,87] The DDPPPA and DDPBA based OLEDs show improved device efficiencies of η_{ex} of 4.72% (5 wt% DDPPPA) and 5.63% (5 wt% DDPBA).[88] The doped device *m*-MTDATA:DDPPPA/*m*-MTDATA:DDPBA show maximum efficiencies of η_c −7.4/8.23 cd A^{-1}; η_p −5.8/6.13 lm W^{-1}; η_{ex} −4.72/5.63%

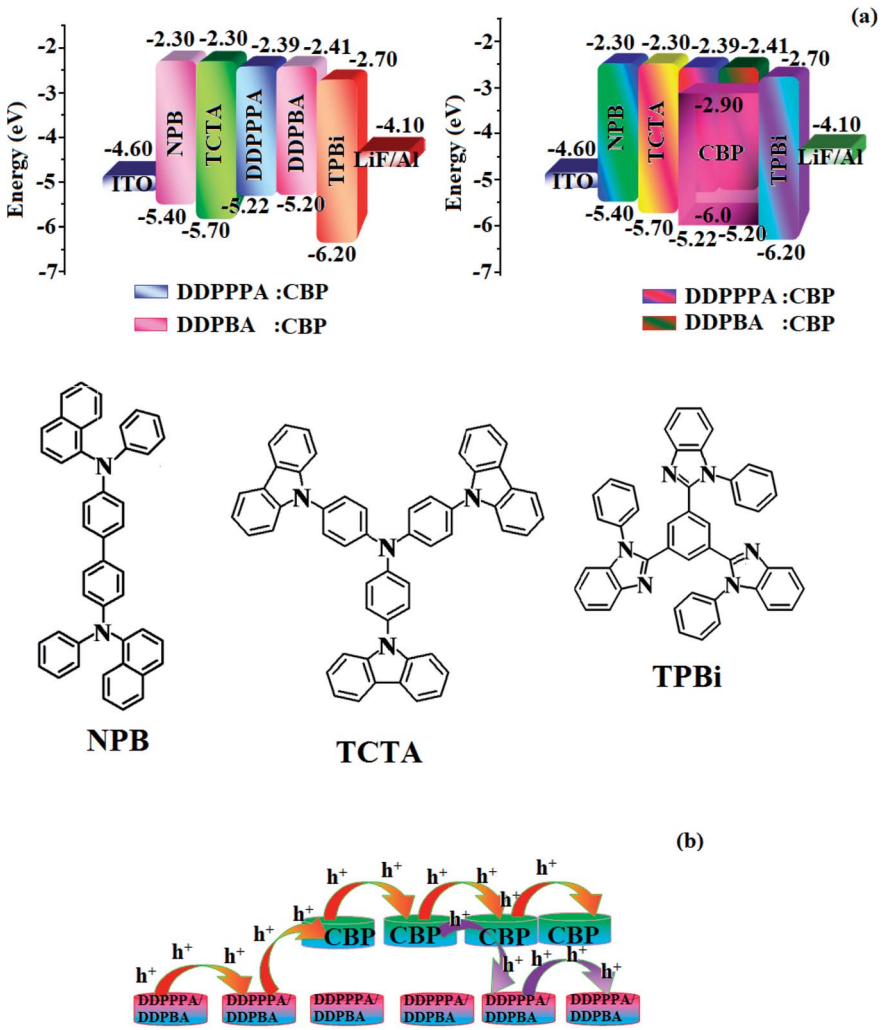

Fig. 5 (a) Schematic representation of energy level diagram of DDPPPA and DDPBA; (b) carrier hopping through both CBP and DDPPPA and DDPBA.

(5 wt%):η_c −8.36/9.15 cd A^{-1}; η_p −6.32/6.65 lm W^{-1}; η_{ex} −4.86/5.45% (10 wt%):η_c −9.58/10.02 cd A^{-1}; η_p −7.8/8.25 lm W^{-1}; η_{ex} −5.96/6.25% (20 wt%). The doped device based on TAPC host TAPC:DDPPPA/TAPC:DDPBA exhibit maximum efficiencies of η_c −9.60/10.03 cd A^{-1}; η_p −7.81/8.26 lm W^{-1}; η_{ex} −5.96/6.25% (20 wt%).

Table 3 Summary of device efficiencies with reported non-doped emitters

Emitter	V_{on} (V)	EL (nm)	η_{ex} (%)	η_c (cd A^{-1})	η_p (lm W^{-1})	CIE (x, y)	Ref.
DDPPPA	**2.3**	**480**	**5.70**	**10.5**	**8.3**	**(0.15, 0.08)**	**This work**
DDPBA	**2.2**	**470**	**6.0**	**12.0**	**9.2**	**(0.15, 0.30)**	**This work**
Py-BPA-BPI	2.15	471	5.64	10.9	10.5	(0.17, 0.29)	18
TPA3HTPE	3.7	471	3.8	6.97	7.99	—	74
DBTO-MeTPE	4.6	481	3.01	6.17	3.82	(0.17, 0.28)	75
DPATPE	3.2	488	3.3	7.5	7.9	—	76
MeTPA-3pTP	3.1	480	3.99	7.04	8.03	(0.17, 0.28)	77
DPF-TPI	2.7	468	4.85	8.41	7.23	(0.17, 0.24)	15
TPATPE	3.6	492	3.4	8.6	5.3	—	79
TPTPE	4.2	488	2.7	5.8	3.5	(0.17, 0.28)	13
TPE-2mTPA	3.6	489	—	4.24	2.10	(0.14, 0.28)	81
Blu2	3.0	—	6.12	11.6	7.23	(0.148, 0.28)	82
PBAPE	6.3	466	—	6.1	3.1	(0.19, 0.27)	83

The theoretically calculated maximum η_{EQE} is of 5.61/5.20% DDPPPA (neat/20 wt% *m*-MDATA) and 5.55/5.10% DDPBA (neat/20 wt% *m*-MDATA) [$\eta_{EQE} = \eta_{out} \times \eta_{rec} \times \eta_{\gamma} \times \Phi_{PL}$,[89] ϕ_{PL}:-DDPPPA (89/96%) and DDPBA (90/98%), η_{out} – out-coupling efficiency (20%), η_{rec} – product of charge recombination efficiency (100%), η_{γ} – radiative exciton-production (25%)] and the experimental η_{EQE} is of 5.70/5.96% DDPPPA (neat/20 wt%) and 6.01/6.25%, DDPBA (neat/20 wt%) respectively. Similar trend is observed by using TAPC as host (experimental η_{EQE}:DDPPPA/DDPBA:TAPC – 5.96/6.25 > theoretical η_{EQE} DDPPPA/DDPBA:TAPC – 5.61/5.56). The experimental η_{EQE} > theoretical η_{EQE} because larger triplet excitons are converted to singlet excitons in EL process.[90–92] The η_r calculated for DDPPPA (neat/20 wt%) (25–31%/27–33%) and DDPBA (neat/20 wt%) (26–31%/27–34%) indicates $\gamma < 100\%$ because of poor unbalanced carrier transportation in the emissive layer. Enhanced η_{IQE} 28/29% (*m*-MTDATA or TAPC:DDPPPA:neat/20 wt%); 30/31% (*m*-MTDATA or TAPC:DDPBA:neat/20 wt%) and maximum η_s of 31.4/32.5% (*m*-MTDATA or TAPC:DDPPPA:neat/20 wt%) and 33.3/34.4% (*m*-MTDATA or TAPC:DDPBA:neat/20 wt%) [$\eta_s = \eta_{out} \times \eta_{PL} \times \eta_{res} \div \eta_{EL}$] is because of retained CT% in D–π–A compounds. Maximum η_s breaking 25% limit: 6.4% (DDPPPA) and 8.3% (DDPBA) of triplet exciton converted to singlet exciton by RISC and remaining follow non-radiative process leads to high efficiency blue OLEDs. These experimental results reveal that non-doped [DDPPPA and DDPBA] and doped [*m*-MTDATA:DDPPPA and *m*-MTDATA:DDPBA] devices are the efficient one. Additional triplet exciton is utilized in the OLEDs because of HLCT of DBTPIN and NDBNPIN as showing the accuracy for our molecular-design-strategy.

4. Conclusion

We have synthesized aromatically substituted phenanthroimidazole at C6 and C9 positions to enhance thermal, photochemical and electroluminescent properties. The intramolecular charge transfer between pyrene moiety at C6/C9 positions and phenanthroimidazole core has been confirmed by experimental and theoretical studies. Photophysical studies reveal that C6 and C9 pyrene substituent induced moderate conjugation relative to C2 modification. The blue device with DDPBA emissive layer show sky blue emission (470 nm, CIE-0.16, 0.10) with maximum efficiencies of η_c −12.0 cd A^{-1}; η_p −9.2 lm W^{-1}; η_{ex} −6.0% at 2.2 V. Both devices show high singlet exciton utilizing efficiency (η_s) of DDPPPA-31.33% and DDPBA-35.29%. The doped device *m*-MTDATA:DDPPPA/*m*-MTDATA:DDPBA show maximum efficiencies of η_c −7.4/8.23 cd A^{-1}; η_p −5.8/6.13 lm W^{-1}; η_{ex} −4.72/5.63% (5 wt%):η_c −8.36/9.15 cd A^{-1}; η_p −6.32/6.65 lm W^{-1}; η_{ex} −4.86/5.45% (10 wt%):η_c −9.58/10.02 cd A^{-1}; η_p −7.8/8.25 lm W^{-1}; η_{ex} −5.96/6.25% (20 wt%). The doped device based on TAPC host TAPC:DDPPPA/TAPC:DDPBA exhibit maximum efficiencies of η_c −9.60/10.03 cd A^{-1}; η_p −7.81/8.26 lm W^{-1}; η_{ex} −5.96/6.25% (20 wt%).

Conflicts of interest

There are no conflicts of interest.

Acknowledgements

This research was supported by the DST (Department of Science and Technology – EMR/2014/000094, F. no. SR/S1/1C-73/2010, F. no. SR/S1/1C-07/2007), DRDO (Defence Research and Development Organization – 213/MAT/10-11), CSIR (Council of Scientific and Industrial Research – no. 01/(2707)/13EMR-II), UGC (University Grant Commission – 6-21/2008, F. no. 30-71/2004(SR)) and DST-Nano Mission (SR/NM/NS-1001/2016).

References

1 C. H. Chen, M. T. Lee and C. H. Liao, *SPIE Newsroom*, 2006.
2 Z. Wang, P. Lu, S. Chen, Z. Gao, F. Shen and W. Zhang, *J. Mater. Chem.*, 2011, **21**, 5451–5457.
3 Z. Jiang, Z. Liu, C. Yang, C. Zhong, J. Qin, G. Yu and Y. Liu, *Adv. Funct. Mater.*, 2009, **19**, 3987–3995.
4 H. H. Chou, Y. H. Chen, H. P. Hsu, W. H. Chang, Y. H. Chen and C. H. Cheng, *Adv. Mater.*, 2012, **24**, 5867–5871.
5 H. Sasabe and J. Kido, *J. Mater. Chem. C*, 2013, **1**, 1699–1707.
6 X. Ouyang, X. L. Li, L. Ai, D. Mi, Z. Ge and S. J. Su, *ACS Appl. Mater. Interfaces*, 2015, **7**, 7869–7877.
7 (*a*) J. Ding, J. Gao, Y. Cheng, Z. Xie, L. Wang, D. Ma, X. Jing and F. Wang, *Adv. Funct. Mater.*, 2006, **16**, 575–581; (*b*) H. Sasabe, J. Takamatsu, T. Motoyama, S. Watanabe, G. Wagenblast, N. Langer, O. Molt, E. Fuchs, C. Lennartz and J. Kido, *Adv. Mater.*, 2010, **22**, 5003–5007; (*c*) M. Zhu and C. Yang, *Chem. Soc. Rev.*, 2013, **42**, 4963–4976; (*d*) T. Fleetham, G. J. Li, L. L. Wen and J. Li, *Adv. Mater.*, 2014, **26**, 7116–7121.
8 (*a*) J. Huang, N. Sun, Y. Dong, R. Tang, P. Lu, P. Cai, Q. Li, D. Ma, J. Qin and Z. Li, *Adv. Funct. Mater.*, 2013, **23**, 2329–2337; (*b*) C. J. Tonzola, A. P. Kulkarni, A. P. Gifford, W. Kaminsky and S. A. Jenekhe, *Adv. Funct. Mater.*, 2007, **17**, 863–874; (*c*) C. H. Chien, C. K. Chen, F. M. Hsu, C. F. Shu, P. T. Chou and C. H. Lai, *Adv. Funct. Mater.*, 2009, **19**, 560–566.
9 M. Zhu and C. Yang, *Chem. Soc. Rev.*, 2013, **42**, 4963–4976.
10 A. Richaud, N. Barba-Behrens and F. Méndez, *Org. Lett.*, 2011, **13**, 972–975.
11 K. Hofmann, *Imidazole and its derivatives*, Inter Science Publishers, Part I Inc., New York, 1953, ISBN: 0-470-37653-8.
12 W. C. Chen, Y. Yuan, G. F. Wu, H. X. Wei, L. Tang, Q. X. Tong, F. L. Wong and C. S. Lee, *Adv. Opt. Mater.*, 2014, **2**, 626–631.
13 W. Li, D. Liu, F. Shen, D. Ma, Z. Wang, T. Feng, Y. Xu, B. Yang and Y. Ma, *Adv. Funct. Mater.*, 2012, **22**, 2797–2803.
14 W. C. Chen, Y. Yuan, S. F. Ni, Z. L. Zhu, J. Zhang, Z. Q. Jiang, L. S. Liao, F. L. Wong and C. S. Lee, *ACS Appl. Mater. Interfaces*, 2017, **9**, 7331–7338.
15 Y. Yuan, J. X. Chen, F. Lu, Q. X. Tong, Q. D. Yang, H. W. Mo, T. W. Ng, F. L. Wong, Z. Q. Guo, J. Ye, Z. Chen, X. H. Zhang and C. S. Lee, *Chem. Mater.*, 2013, **25**, 4957–4965.
16 Y. Zhang, J. H. Wang, G. Han, F. Lu and Q. X. Tong, *RSC Adv.*, 2016, **6**, 70800–70809.
17 M. Chen, Y. Yuan, J. Zheng, W. C. Chen, L. J. Shi, Z. Zhu, L. F. Lu, Q. X. Tong, Q. D. Yang, J. Ye, M. Y. Chan and C. S. Lee, *Adv. Opt. Mater.*, 2015, **3**, 1215–1219.

18 B. Liu, Y. Yuan, D. He, D. Y. Huang, C. Y. Luo, Z. L. Zhu, F. Lu, Q. X. Tong and C. S. Lee, *Chem.–Eur. J.*, 2016, **22**, 12130–12137.

19 D. He, Y. Yuan, B. Liu, D. Y. Huang, C. Y. Luo, F. Lu, Q. X. Tong and C. S. Lee, *Dyes Pigm.*, 2017, **136**, 347–353.

20 (*a*) S. Jeong and J. I. Hong, *Dyes Pigm.*, 2017, **144**, 9–16; (*b*) A. Islam, Q. Wang, L. Zhang, T. Lei, L. Hong, R. Yang, Z. Liu, R. Peng, L. S. Liao and Z. Ge, *Dyes Pigm.*, 2017, **142**, 499–506.

21 Y. Park, J. H. Lee, D. H. Jung, S. H. Liu, Y. H. Lin and L. Y. Chen, *J. Mater. Chem.*, 2010, **20**, 5930–5936.

22 Z. X. Wang, H. X. Shao, J. C. Ye, L. Zhang and P. Lu, *Adv. Funct. Mater.*, 2007, **17**, 253–263.

23 S. Tao, Y. Zhou, C. S. Lee, S. T. Lee, D. Huang and X. Zhang, *J. Phys. Chem. C*, 2008, **112**, 14603–14606.

24 S. K. Kim, B. Yang, Y. I. Park, Y. Ma, J. Y. Lee, H. J. Kim and J. Park, *Org. Electron.*, 2009, **10**, 822–833.

25 W. Li, D. Liu, F. Shen, D. Ma, Z. Wang, T. Feng, Y. Xu, B. Yang and Y. Ma, *Adv. Funct. Mater.*, 2012, **22**, 2797–2803.

26 L. Yao, S. Zhang, R. Wang, W. Li, F. Shen, B. Yang and Y. Ma, *Angew. Chem., Int. Ed.*, 2014, **53**, 2119–2123.

27 S. K. Kim, B. Yang, Y. Ma, J. H. Lee and J.-W. Park, *J. Mater. Chem.*, 2008, **18**, 3376–3384.

28 H. Liu, Q. Bai, L. Yao, H. Zhang, H. Xu, S. Zhang, W. Li, Y. Gao, J. Li, P. Lu, H. Wang, B. Yang and Y. Mac, *Chem. Sci.*, 2015, **6**, 3797–3804.

29 H. Wang, L. Xie, Q. Peng, L. Meng, Y. Wang, Y. Yi and P. Wang, *Adv. Mater.*, 2014, **26**, 5198–5204.

30 Z. Wu, J. Luo, N. Sun, L. Zhu, H. Sun, L. Yu, D. Yang, X. Qiao, J. Chen, C. Yang and D. Ma, *Adv. Funct. Mater.*, 2016, **26**, 3306–3313.

31 W. Li, Y. Pan, L. Yao, H. Liu, S. Zhang, C. Wang, F. Shen, P. Lu, B. Yang and Y. Ma, *Adv. Opt. Mater.*, 2014, **2**, 892–901.

32 Q. Zhang, B. Li, S. Huang, H. Nomura, H. Tanaka and C. Adachi, *Nat. Photonics*, 2014, **8**, 326–332.

33 S. Y. Lee, T. Yasuda, H. Nomura and C. Adachi, *Appl. Phys. Lett.*, 2012, **101**, 093306.

34 H. Tanaka, K. Shizu, H. Miyazaki and C. Adachi, *Chem. Commun.*, 2012, **48**, 11392–11394.

35 T. Nakagawa, S.-Y. Ku, K.-T. Wong and C. Adachi, *Chem. Commun.*, 2012, **48**, 9580–9582.

36 W. J. Li, Y. Y. Pan, R. Xiao, Q. M. Peng, S. T. Zhang, D. G. Ma, F. Li, F. Z. Shen, Y. H. Wang, B. Yang and Y. G. Ma, *Adv. Funct. Mater.*, 2014, **24**, 1609–1614.

37 S. Tang, W. J. Li, F. Z. Shen, D. D. Liu, B. Yang and Y. G. Ma, *J. Mater. Chem.*, 2012, **22**, 4401–4408.

38 S. T. Zhang, W. J. Li, L. Yao, Y. Y. Pan, B. Yang and Y. G. Ma, *Chem. Commun.*, 2013, **49**, 11302–11304.

39 L. Yao, S. T. Zhang, R. Wang, W. J. Li, F. Z. Shen, B. Yang and Y. G. Ma, *Angew. Chem., Int. Ed.*, 2014, **53**, 2119–2123.

40 Y. Y. Pan, W. J. Li, S. T. Zhang, L. Yao, C. Gu, H. Xu, B. Yang and Y. G. Ma, *Adv. Opt. Mater.*, 2014, **2**, 510–515.

41 W. J. Li, Y. Y. Pan, L. Yao, H. C. Liu, S. T. Zhang, C. Wang, F. Z. Shen, B. Yang and G. A. Ma, *Adv. Opt. Mater.*, 2014, **2**, 892–901.

42 D. Chaudhuri, E. Sigmund, A. Meyer, L. Rcck, P. Klemm, S. Lautenschlager, A. Schmid, S. R. Yost, T. Van, S. Bange, S. Hcger and J. M. Lupton, *Angew. Chem.*, 2013, **52**, 13449–13452.

43 J. R. Sheats, H. Antoniadis, M. Hueschen, W. Leonard, J. Miller, R. Moon and D. Roitman, *Science*, 1996, **273**, 884–888.

44 T. Forster, *Discuss. Faraday Soc.*, 1959, **27**, 7–17.

45 S. Zhang, L. Yao, Q. Peng, W. Li, Y. Pan, R. Xiao, Y. Gao, C. Gu, Z. Wang, P. Lu, F. Li, S. Su, B. Yang and Y. Ma, *Adv. Funct. Mater.*, 2015, **25**, 1755–1762.

46 (*a*) M. J. Frisch, G. W. Trucks, H. B. Schlegel, G. E. Scuseria, M. A. Robb, J. R. Cheeseman, G. Scalmani, V. Barone, B. Mennucci, G. A. Petersson, H. Nakatsuji, M. Caricato, X. Li, H. P. Hratchian, A. F. Izmaylov, J. Bloino, G. Zheng, J. L. Sonnenberg, M. Hada, M. Ehara, K. Toyota, R. Fukuda, J. Hasegawa, M. Ishida, T. Nakajima, Y. Honda, O. Kitao, H. Nakai, T. Vreven, J. A. Montgomery, J. E. Peralta, F. Ogliaro, M. Bearpark, J. J. Heyd, E. Brothers, K. N. Kudin, V. N. Staroverov, R. Kobayashi, J. Normand, K. Raghavachari, A. Rendell, J. C. Burant, S. S. Iyengar, J. Tomasi, M. Cossi, N. Rega, J. M. Millam, M. Klene, J. E. Knox, J. B. Cross, V. Bakken, C. Adamo, J. Jaramillo, R. Gomperts, R. E. Stratmann, O. Yazyev, A. J. Austin, R. Cammi, C. Pomelli, J. W. Ochterski, R. L. Martin, K. Morokuma, V. G. Zakrzewski, G. A. Voth, P. Salvador, J. J. Dannenberg, S. Dapprich, A. D. Daniels, O. Farkas, J. B. Foresman, J. V. Ortiz, J. Cioslowski and D. J. Fox, *Revision A.02*, Gaussian, Inc., Wallingford, CT, 2009; (*b*) T. Lu and F. Chen, *J. Comput. Chem.*, 2012, **33**, 580–592.

47 S. Zhang, L. Yao, Q. Peng, W. Li, Y. Pan, R. Xiao, Y. Gao, C. Gu, Z. Wang, P. Lu, F. Li, S. Su, B. Yang and Y. Ma, *Adv. Funct. Mater.*, 2015, **25**, 1755–1762.

48 M. A. Baldo, S. Lamansky, P. E. Burrows, M. E. Thompson and S. R. Forrest, *Appl. Phys. Lett.*, 1999, **60**, 14422–14428.

49 Y. Tao, Q. Wang, C. Yang, Q. Wang, Z. Zhang and T. Zou, *Angew. Chem.*, 2008, **47**, 8104–8107.

50 W. C. Chen, Y. Yuan, G. F. Wu, H. X. Wei, J. Ye, M. Chen, F. Lu, Q. X. Tong, F. L. Wong and C. S. Lee, *Org. Electron.*, 2015, **17**, 159–166.

51 R. L. Martin, *J. Chem. Phys.*, 2003, **118**, 4775–4777.

52 S. Tretiak and S. Mukamel, *Chem. Rev.*, 2002, **102**, 3171–3212.

53 (*a*) C. J. Kuo, T. Y. Li, C. C. Lien, C. H. Liu, F. I. Wu and M. J. Huang, *J. Mater. Chem.*, 2009, **19**, 1865–1871; (*b*) Z. M. Wang, P. Lu, S. M. Chen, Z. Gao, F. Z. Shen, W. S. Zhang, Y. X. Xu, H. S. Kwok and Y. G. Ma, *J. Mater. Chem.*, 2011, **21**, 5451–5456; (*c*) W. J. Li, D. D. Liu, F. Z. Shen, D. G. Ma, Z. M. Wang, T. Feng, Y. X. Xu, B. Yang and Y. G. Ma, *Adv. Funct. Mater.*, 2012, **22**, 2797–2803; (*d*) K. Wang, F. C. Zhao, C. G. Wang, S. Y. Chen, D. Chen, H. Y. Zhang, Y. Liu, D. G. Ma and Y. Wang, *Adv. Funct. Mater.*, 2013, **23**, 2672–2680; (*e*) W. C. Chen, Y. Yuan, G. F. Wu, H. X. Wei, L. Tang, Q. X. Tong, F. L. Wong and C. S. Lee, *Adv. Opt. Mater.*, 2014, **2**, 626–631; (*f*) W. C. Chen, Q. X. Tong and C. S. Lee, *J. Mater. Chem. C*, 2015, **3**, 10957–10963; (*g*) C. Li, S. Wang, W. Chen, J. Wei, G. Yang, K. Ye, Y. Liu and Y. Wang,

Chem. Commun., 2015, **51**, 10632–10635; (*h*) W. C. Chen, Y. Yuan, G. F. Wu, H. X. Wei, J. Ye, M. Chen, Q. X. Lu, F. Tong, F. L. Wong and C. S. Lee, *Org. Electron.*, 2015, **17**, 159–166; (*i*) L. Bin, J. W. Zhao, C. Y. Luo, L. Feng, S. L. Tao and Q. X. Tong, *J. Mater. Chem. C*, 2016, **4**, 2003–2010.

54 (*a*) J. Ye, Z. Chen, M. K. Fung, C. Zheng, X. Ou, X. Zhang, Y. Yuan and C. S. Lee, *Chem. Mater.*, 2013, **25**, 2630–2637; (*b*) Y. C. Li, Z. H. Wang, X. L. Li, G. Z. Xie, D. C. Chen, Y. F. Wang, C. C. Lo, A. Lien, J. B. Peng, Y. Cao and S. J. Su, *Chem. Mater.*, 2015, **27**, 1100–1109; (*c*) R. Hu, E. Lager, A. A. Aguilar, J. Z. Liu, J. W. Y. Lam, H. H. Y. Sung, I. D. Williams, Y. C. Zhong, K. S. Wong, E. Pena-Cabrera and B. Z. Tang, *J. Phys. Chem. A*, 2009, **113**, 15845–15853.

55 (*a*) Y. Zhang, S. L. Lai, Q. X. Tong, M. F. Lo, T. W. Ng, M. Y. Chan, Z. C. Wen, J. He, K. S. Jeff, X. L. Tang, W. M. Liu, C. C. Ko, P. F. Wang and C. S. Lee, *Chem. Mater.*, 2012, **24**, 61–70; (*b*) C. Chen, Y. Yuan, Y. Xiong, A. L. Rogach, Q. X. Tong and C.-S. Lee, *ACS Appl. Mater. Interfaces*, 2017, **9**, 26268–26278.

56 S. Zhuang, R. Shangguan, H. Huang, G. Tua, L. Wang and X. Zhu, *Dyes Pigm.*, 2014, **101**, 93–102.

57 Z. Ma, E. Wang, M. E. Jarvid, P. Henriksson, O. Inganas, F. Zhang and M. R. Andersson, *J. Mater. Chem.*, 2012, **22**, 2306–2314.

58 (*a*) W. J. Li, D. D. Liu, F. Z. Shen, D. G. Ma, Z. M. Wang, T. Feng, Y. X. Xu, B. Yang and Y. G. Ma, *Adv. Funct. Mater.*, 2012, **22**, 2797–2803; (*b*) G. B. Bodedla, K. R. Justin Thomas, M.-S. Fan and K.-C. Ho, *J. Org. Chem.*, 2016, **81**, 640–653.

59 X. Chen, G. Zhang, H. Luo, Y. Li, Z. Liu and D. Zhang, *J. Mater. Chem. C*, 2014, **2**, 2869–2876.

60 (*a*) G. M. Li, D. X. Zhu, T. Peng, Y. Liu, Y. Wang and M. R. Bryce, *Adv. Funct. Mater.*, 2014, **24**, 7420–7426; (*b*) Y. T. Tao, Q. Wang, C. L. Yang, C. Zhong, K. Zhang, J. G. Qin and D. G. Ma, *Adv. Funct. Mater.*, 2010, **20**, 304–311; (*c*) H. Liu, P. Chen, D. H. Hu, X. Y. Tang, Y. Y. Pan, H. H. Zhang, W. Q. Zhang, X. Han, Q. Bai, P. Lu and Y. G. Ma, *Chem.–Eur. J.*, 2014, **86**, 7286–7292; (*d*) D. H. Hu, F. Z. Shen, H. Liu, P. Lu, Y. Lv, D. D. Liu and Y. G. Ma, *Chem. Commun.*, 2012, **48**, 3015–3017.

61 M. R. Zhu and C. L. Yang, *Chem. Soc. Rev.*, 2013, **42**, 4963–4976.

62 H. H. Chou, Y. H. Chen, H. P. Hsu, W. H. Chang, Y. H. Chen and C. H. Cheng, *Adv. Mater.*, 2012, **24**, 5867–5871.

63 Q. Zhang, J. Li, K. Shizu, S. Huang, S. Hirata, H. Miyazaki and C. Adachi, *J. Am. Chem. Soc.*, 2012, **134**, 14706–14709.

64 (*a*) M. Segal, M. Singh, K. Rivoir, S. Difley, T. V. Voorhis and M. A. Baldo, *Nat. Mater.*, 2007, **6**, 374–378; (*b*) W. Barford, *Phys. Rev. B: Condens. Matter Mater. Phys.*, 2004, **70**, 205204–205212.

65 W. Jiang, L. Duan, J. Qiao, G. Dong, L. Wang and Y. Qiu, *Org. Lett.*, 2011, **13**, 3146–3149.

66 Y. Tao, Q. Wang, C. Yang, C. Zhong, K. Zhang, J. Ma and D. Qin, *Adv. Funct. Mater.*, 2010, **20**, 304–311.

67 Y. Liu, L. S. Cui, M. F. Xu, X. B. Shi, X. B. Zhou, Z. K. Wang, Z. Q. Jiang and L. S. Liao, *J. Mater. Chem. C*, 2014, **2**, 2488–2495.

68 Y. H. Lou, M. F. Xu, L. Zhang, Z. K. Wang, S. Naka, H. Okada and L. S. Liao, *Org. Electron.*, 2013, **14**, 2698–2704.

69 Z. Wang, Y. Lou, S. Naka and H. Okada, *Appl. Phys. Lett.*, 2011, **98**, 063302–063306.

70 R. R. Hu, E. Lager, A. L. Aguilar-Aguilar, J. Z. Liu, J. W. Y. Lam, H. H. Y. Sung, I. D. Williams, Y. C. Zhong, K. S. Wong, E. Pena-Cabrera and B. Z. Tang, *J. Phys. Chem. A*, 2009, **113**, 15845–15853.

71 (*a*) Y. P. Li, F. Li, H. Y. Zhang, Z. Q. Xie, W. J. Xie, H. Xu, B. Li, F. Z. Shen, L. Ye, M. Hanif, D. G. Ma and Y. G. Ma, *Chem. Commun.*, 2007, 231–233; (*b*) Y. P. Li, F. Z. Shen, H. Wang, F. He, Z. Q. Xie, H. Y. Zhang, Z. M. Wang, L. L. Liu, F. Li, M. Hanif, L. Ye and L. Ma, *Chem. Mater.*, 2008, **20**, 7312–7318.

72 (*a*) S. T. Zhang, W. J. Li, L. Yao, Y. Y. Pan, F. Z. Shen, R. Xiao, B. Yang and Y. G. Ma, *Chem. Commun.*, 2013, **49**, 11302–11304; (*b*) C. Cao, W. C. Chen, J. X. Chen, L. Yang, X. Z. Wang, H. Yang, B. Huang, Z. L. Zhu, Q. X. Tong and C. S. Lee, *ACS Appl. Mater. Interfaces*, 2019, **11**, 11691–11698; (*c*) H. C. Liu, Q. Bai, L. Yao, H. Y. Zhang, H. Xu, S. T. Zhang, W. J. Li, Y. Gao, J. Y. Li, P. Lu, H. Y. Wang, B. Yang and Y. G. Ma, *Chem. Sci.*, 2015, **6**, 4623–4635; (*d*) X. Y. Tang, Q. Bai, Q. M. Peng, Y. Gao, J. Y. Li, Y. L. Liu, L. Yao, P. Lu, B. Yang and Y. G. Ma, *Chem. Mater.*, 2015, **27**, 7050–7057; (*e*) Q. Zhang, D. Tsang, H. Kuwabara, Y. Hatae, B. Li, T. Takahashi, S. Y. Lee, T. Yasuda and C. Adachi, *Adv. Mater.*, 2015, **27**, 2096–2100.

73 B. Liu, Y. Yuan, D. He, D. Y. Huang, C. Y. Luo, Z. L. Zhu, F. Lu, Q. X. Tong and C. S. Lee, *Chem.–Eur. J.*, 2016, **22**, 12130–12137.

74 G. Chen, W. Li, T. Zhou, Q. Peng, D. Zhai, H. Li, W. Z. Yuan, Y. Zhang and B. Z. Tang, *Adv. Mater.*, 2015, **27**, 4496–4501.

75 L. Zhan, S. Wang, L. X. Ding, Z. Li and H. Wang, *J. Mater. Chem. C*, 2015, **3**, 19711–19717.

76 C. Y. K. Chan, J. W. Y. Lam, Z. Zhao, S. Chen, P. Lu, H. H. Y. Sung, H. S. Kwok, Y. Ma, I. D. Williams and B. Z. Tang, *J. Mater. Chem. C*, 2014, **2**, 4320–4327.

77 J. Huang, N. Sun, J. Yang, R. Tang, Q. Li, D. Ma and Z. Li, *Adv. Funct. Mater.*, 2014, **24**, 7645–7654.

78 (*a*) C. Cao, W. C. Chen, S. Tian, J. X. Chen, Z. Y. Wang, X. H. Zheng, C. W. Ding, J. H. Li, J. J. Zhu, Z. L. Zhu, Q. X. Tong and C. S. Lee, *Mater. Chem. Front.*, 2019, **3**, 1071–1079; (*b*) X. H. Zheng, J. W. Zhao, T. T. Huang, X. Chen, C. Cao, G. X. Yang, Z. H. Lin, Q. X. Tong, S. L. Tao and D. Liu, *ChemElectroChem*, 2019, **6**, 5810–5818.

79 Y. Liu, S. Chen, J. W. Y. Lam, P. Lu, R. T. K. Kwok, F. Mahtab, H. S. Kwok and B. Z. Tang, *Chem. Mater.*, 2011, **23**, 2536–2544.

80 C. Y. K. Chan, Z. Zhao, J. W. Y. Lam, J. Liu, S. Chen, P. Lu, F. Mahtab, X. Chen, H. H. Y. Sung, H. S. Kwok, Y. Ma, I. D. Williams, K. S. Wong and B. Z. Tang, *Adv. Funct. Mater.*, 2012, **22**, 378–389.

81 J. Huang, R. Tang, T. Zhang, Q. Li, G. Yu, S. Xie, Y. Liu, S. Ye, J. Qin and Z. Li, *Chem.–Eur. J.*, 2014, **20**, 5317–5326.

82 C. G. Zhen, Y. F. Dai, W. J. Zeng, Z. Z. K. Chen and J. Kieffer, *Adv. Funct. Mater.*, 2011, **21**, 699–707.
83 S. K. Kim, Y. Park, I. Kang and J. Park, *J. Mater. Chem.*, 2007, **17**, 4670–4678.
84 H. Uoyama, K. Goushi, K. Shizu, H. Nomura and C. Adachi, *Nature*, 2012, **492**, 234–238.
85 (*a*) R. Butkute, R. Lygaitis, V. Mimaite, D. Gudeika, D. Volyniuk, G. Sini and J. V. Grazulevicius, *Dyes Pigm.*, 2017, **146**, 425–437; (*b*) T. Zhang, B. Chu, W. Li, Z. Su, Q. M. Peng, B. Zhao, Y. Luo, F. Jin, X. Yan, Y. Gao, H. Wu, F. Zhang, D. Fan and J. Wang, *ACS Appl. Mater. Interfaces*, 2014, **6**, 11907–11921; (*c*) D. Chen, Z. Wang, D. Wang, Y. C. Wu, C. Lo, A. Lien, Y. Cao and S. J. Su, *Org. Electron.*, 2015, **25**, 79–84.
86 G. Xie, D. Chen, X. Li, X. Cai, Y. Li, D. Chen, K. Liu, Q. Zhang, Y. Cao and S. J. Su, *ACS Appl. Mater. Interfaces*, 2016, **8**, 27920–27930.
87 J. H. Jou, Y. L. Chen, J. R. Tseng, R. Z. Wu, J. J. Shyue, K. R. Justin Thomas, N. Kapoor, C. T. Chen, Y. P. Lin, P. H. Wang, H. W. Hung, J. Y. Li and S. P. Chen, *J. Mater. Chem.*, 2012, **22**, 15500–15506.
88 W. C. Chen, Y. Yuan, G. F. Wu, H. X. Wei, J. Ye, M. Chen, F. Lu, Q. X. Tong, F. L. Wong and C. S. Lee, *Org. Electron.*, 2015, **17**, 159–166.
89 S. H. Cho, J. R. Oh, H. K. Park, H. K. Kim, Y. H. Lee, J. G. Lee and Y. R. Do, *Opt. Express*, 2010, **18**, 1099–1104.
90 M. Zhu and C. Yang, *Chem. Soc. Rev.*, 2013, **42**, 4963–4976.
91 W. C. Chen, Q. X. Tong and C. S. Lee, *Sci. Adv. Mater.*, 2015, **7**, 2193–2205.
92 Y. Xu, X. Liang, X. Zhou, P. Yuan, J. Zhou, C. Wang, B. Li, D. Hu, X. Qiao, X. Jiang, L. Liu, S. J. Su, D. Ma and Y. Ma, *Adv. Mater.*, 2019, **31**, 1807388–1807396.